Article

Double-Diffusive Effects on the Onset of Rayleigh-Benard Convection of Water-Based Nanofluids

Massimo Corcione (ID) **and Alessandro Quintino** * (ID)

DIAEE, Sapienza Università di Roma, Via Eudossiana 18, 00184 Roma, Italy
* Correspondence: alessandro.quintino@uniroma1.it

Abstract: A numerical study on the Rayleigh–Benard convection in a shallow cavity filled with different metal-oxide water-based nanofluids is presented through a two-phase model, which accounts for the effects of the Brownian diffusion and thermophoresis, at variable properties with temperature. Numerical simulations are executed for different values of the average volume fraction of the nanoparticles, different aspect ratios of the enclosure, as well as for temperature difference between the bottom and the top walls. It is found that the dispersion of the nanoparticle into the base fluid increases the stability of the nanofluid layer, determining the conditions for the onset of convection also with reference to the confinement of the nanofluid.

Keywords: nanofluids; Rayleigh–Benard convection; onset of convection; critical Rayleigh number

1. Introduction

The thermal instability of a horizontal nanofluid layer, confined between rigid boundaries and heated from below, has been the subject of several theoretical and numerical studies, for its importance in particular engineering applications, as the cooling of the micro-electronic devices and the solar collectors. However, a number of discrepancies can be found mainly due to the different numerical models used, which basically means single-phase or two-phase approaches assuming either physical properties that are variable or constant with temperature. The common evidence is that the addition of nanoparticles to a base fluid has the effect of increasing the dynamic viscosity of the suspension and, consequently, making the layer more stable. This could be reasonable should the nanofluid behave as a single-phase fluid. On the contrary, since the nanofluid actually behaves as a two-phase fluid, the nanoparticle's motion due to the Brownian diffusion and thermophoresis may induce a concentration gradient which enhances the nanofluid layer's instability, even if the Rayleigh number does not exceed the critical Rayleigh number Ra_c for the onset of convection in a pure fluid.

Nanofluid instability due to the aggregation and sedimentation of nanoparticles was observed experimentally by Wen and Ding [1] in a water layer heated from below with the addition of different amounts of TiO_2 nanoparticles. Moreover, although the extra-buoyancy force consequent to the large density difference existing between the solid and liquid phases should lead to a convection enhancement, they measured a heat transfer rate which decreased as the volume fraction was increased, probably as a result of the increase in the effective dynamic viscosity. A totally different result was found by Rao and Srivastava [2], who conducted experiments using a rectangular cavity filled with Al_2O_3 + H_2O, in which significant enhancements of the heat transfer coefficient up to 36% were detected with respect to the base fluid. In their experimental work, Chang et al. [3] suggested that the critical Rayleigh number for the onset of convection of a horizontal colloidal suspension layer heated from below may be strictly related to the size of the suspended particles, whose increase above 100 nm should play a stabilizing effect. On the other hand, when the particle size is smaller than 100 nm, Brownian motion and thermophoresis effects are

sufficient to destabilize the layer. However, the experimental measurement of the critical Rayleigh number represents a very difficult task for the extremely long waiting time needed for perturbations for growing and breaking the nanofluid stratification; thus, an accurate investigation can be obtained only by means of a theoretical stability analysis, in the case of an indefinite horizontal layer, or in a finite-volume numerical simulation if the nanofluid is confined within a cavity, provided that the effective properties are correctly evaluated and the concentration boundary conditions are properly imposed.

The heat transfer features inside a horizontal rectangular cavity filled with alumina-water nanofluids was investigated analytically by Hwang et al. [4] under the hypothesis that the nanofluid behaves as a single-phase fluid. In their model, the Jang–Choi correlation for the thermal conductivity [5] and the Pak–Cho correlation for the dynamic viscosity [6] were used to evaluate the Rayleigh and Prandtl numbers as functions of the mean temperature, the nanofluid volume fraction, and the size of the nanoparticles. They found that the heat transfer rate decreased as the volume fraction was increased and that the nanofluid is more stable than the base fluid. The same results were also obtained by Park [7] using a finite volume method to simulate a cavity filled with $Al_2O_3 + H_2O$, and by Kim at al. [8], using theoretical approaches according to which a little addition of nanoparticles stabilized the fluid layer and simultaneously increased the heat transfer rate.

Completely opposite results have been obtained by Tzou [9,10], who performed a thermal instability analysis using a two-phase model including the nanoparticle diffusion due to Brownian motion and thermophoresis. Although the nanofluid properties were assumed to be constant with temperature, and the thermophoretic diffusion coefficient was extrapolated by the McNab–Meisen equation [11], valid only for particles greater than 1 μm, the resulting critical Rayleigh number was found to be smaller by about two orders of magnitude with respect to the base liquid, and as a consequence of the destabilizing effect due to the nanoparticle diffusion, the heat transfer rate further increased. Smaller values of the critical Rayleigh number for a binary fluid mixture heated from below were also reported in the work of Ryskin et al. [12], in which convective perturbations were found to grow at an effective Rayleigh number well below the critical Rayleigh number for the pure fluid.

The stability of a horizontal nanofluid layer heated from below has been widely investigated too by Nield and Kuznetsov [13–16] with a double-diffusive perturbation technique, which takes in account the Brownian diffusion and thermophoresis. Their results show that the instability of the nanofluid layer increased as the Lewis number increases, being related to a major concentration of heavy nanoparticles in the upper part of the layer due to the opposite temperature gradient. Similar results have been pointed out by Agarwal et al. [17], though the value of the Lewis number considered in their investigation is too small to be representative of the behavior of a nanofluid.

Finally, the few numerical works available in the literature on the thermal convection of nanofluids in cavities including the Brownian diffusion and thermophoresis show that the presence of nanoparticles in the base fluid affects the flow features and the heat transfer but has a negligible effect on the onset conditions [18–22]. In addition to these, many other works numerically analyzed the Rayleigh–Benard convection of nanofluids in cavities with a single-phase approach, yet they are not cited here, being out of the scope of the present work. However, for a comprehensive review on the Rayleigh–Benard instability in nanofluids, the article of Ahuja and Sharma [23] is recommended.

In all cited works, results have been presented in the classical Nu-Ra distributions, in which the dimensionless parameters have been calculate at average values of fluid thermophysical properties. This kind of representation is very exhaustive for describing the thermal performance of a fluid when its properties are not significantly affected by other variables of the system. In the case of nanofluids, in which the effective thermal conductivity and dynamic viscosity are extremely dependent on temperature and volume fraction, the dimensionless comparison between base fluid and nanofluid could lead to erroneous findings, so an analysis in dimension form could be more appropriate.

In the following sections, a numerical study on the Rayleigh–Benard convection in a shallow cavity filled with different metal-oxide water-based nanofluids is presented through a two-phase model, which accounts for the effects of the Brownian diffusion and thermophoresis, at variable properties with temperature. The study is conducted using the average volume fraction and the diameter of the nanoparticles, the temperature difference imposed between the bottom and top surfaces of the cavity, the average nanofluid temperature, and the aspect ratio of the cavity as controlling parameters. Main scope of the study is to delineate the basic heat, mass, and fluid flow features and to analyze how much the stability of a nanofluid is affected by the presence of the nanoparticles dispersed into the base fluid, determining the effective critical Rayleigh number Ra_c also with reference to the confinement of the nanofluid.

2. Materials and Methods

2.1. Mathematical Formulation

Consider a two-dimensional rectangular enclosure of height H and width W, filled with a nanofluid. The bottom of the enclosure is heated at a uniform temperature T_h, while the top is cooled at a uniform temperature T_c, both sidewalls of the cavity being adiabatic, as depicted in Figure 1. The resulting flow is laminar, with negligible pressure work and viscous dissipation. It is assumed that Brownian and thermophoresis diffusion are the only significant slip mechanisms acting between nanoparticles and base fluid, as already discussed by Buongiorno [24]. The thermophysical properties of base fluid vary with temperature and are dependent on the local mass fraction of the suspended solid phase. Radiative heat transfer, as well as the Dufour effect, are neglected.
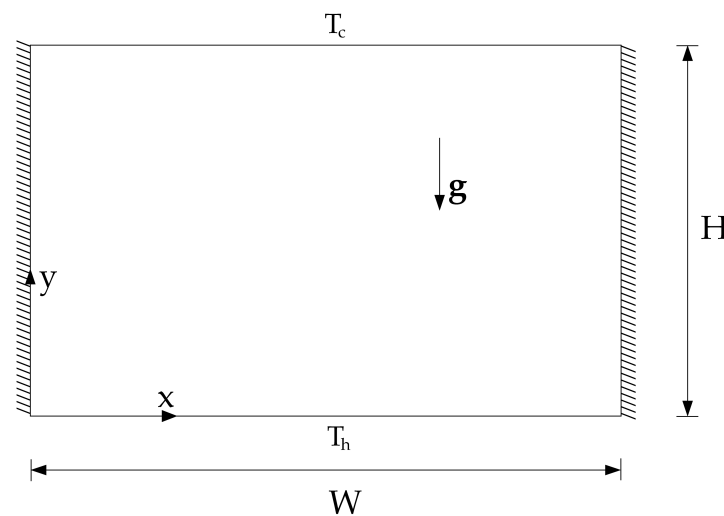

Figure 1. Geometry and coordinate system.

With these hypotheses, the system of governing equations reduce to:

$$\frac{\partial \rho_n}{\partial t} + \nabla \cdot (\rho_n \mathbf{V}) = 0 \tag{1}$$

$$\frac{\partial (\rho_n \mathbf{V})}{\partial t} + \nabla \cdot (\rho_n \mathbf{V}\mathbf{V}) = \nabla \cdot \boldsymbol{\tau} + \rho_n \mathbf{g} \tag{2}$$

$$\frac{\partial (\rho_n c_n T)}{\partial t} + \nabla \cdot (\rho_n \mathbf{V} c_n T) = \nabla \cdot (k_n \nabla T) \tag{3}$$

$$\frac{\partial (\rho_n m)}{\partial t} + \nabla \cdot (\rho_n \mathbf{V} m) = -\nabla \cdot \mathbf{J}_p \tag{4}$$

where t is the time, $\mathbf{V}$ is the velocity vector, $\mathbf{J}_p$ is the nanoparticle diffusion mass flux, m is the mass fraction of the solid phase, and k_n is the nanofluid thermal conductivity. As

demonstrated by several researchers [25–30], the nanofluid is considered to behave as a Newtonian fluid, and thus the stress tensor can be expressed as:

$$\boldsymbol{\tau} = -(p + \frac{2}{3}\mu_n \nabla \cdot \mathbf{V})\mathbf{I} + \mu_n[\nabla \mathbf{V} + (\nabla \mathbf{V}^t)] \tag{5}$$

where μ_n is the effective dynamic viscosity. The nanoparticle diffusion mass flux is given by the sum of Brownian and thermophoretic contributions, and it is expressed by:

$$\mathbf{J}_p = -\rho_n(D_B \nabla m + D_T \frac{\nabla T}{T}) \tag{6}$$

in which D_B and D_T represent the Brownian and thermophoretic diffusion coefficients. The Brownian diffusion coefficient, D_B, is evaluated through the well-known Stokes–Einstein equation [31]:

$$D_B = \frac{\kappa_b T}{3\pi\mu_f d_p} \tag{7}$$

where μ_f and d_p are, respectively, the dynamic viscosity of the base fluid and the diameter of the suspended nanoparticles, and $\kappa_b = 1.38066 \times 10^{-23}$ J/K is the Boltzmann constant. As derived by Brenner and Bielenberg [32], the thermophoretic diffusion coefficient, D_T, is expressed as:

$$D_T = S_T \frac{\mu_f}{\rho_f} m \tag{8}$$

where the value of the thermophoresis parameter, S_T, is calculated by the following correlation proposed by Corcione et al. [33]:

$$S_T = \left[(1.5 \times 10^4)\left(\frac{k_s}{k_f}\right)^{-3} + 0.9\right] \cdot [-16(\varphi_{av})^{2.35} + 0.0195] \tag{9}$$

where k_s, k_f, and φ_{av} represent, respectively, the thermal conductivities of the nanoparticles and of the base fluid and the volume fraction of the suspended solid phase. The prediction of the effective thermophysical properties of nanofluid can be made using the following correlations developed by Corcione [34]:

$$\frac{k_n}{k_f} = 1 + 4.4Re_p^{0.4}Pr_f^{0.66}\left(\frac{T}{T_{fr}}\right)^{10}\left(\frac{k_s}{k_f}\right)^{0.03}\varphi^{0.66} \tag{10}$$

$$\frac{\mu_n}{\mu_f} = \frac{1}{1 - 34.87(\frac{d_p}{d_f})^{-0.3}\varphi^{1.03}} \tag{11}$$

As demonstrated by several research groups [25–30], the nanofluid mass density, ρ_n, and the specific heat at constant pressure, c_n, are calculated by the following expressions:

$$\rho_n = (1 - \varphi)\rho_f + \varphi\rho_s \tag{12}$$

$$c_n = \frac{(1 - \varphi)(\rho c)_f + \varphi(\rho c)_s}{(1 - \varphi)\rho_f + \varphi\rho_s} \tag{13}$$

The temperature-dependence of the generic physical property of the base fluid is approximated as a fourth-order polynomial function obtained by the fit of the data extracted from the NIST Chemistry WebBook [35], whereas the physical properties of nanoparticles, Al$_2$O$_3$, CuO and TiO$_2$, are shown in Table 1.

The assigned boundary conditions are: (a) $T = T_h$, $\mathbf{V} = 0$ and $\mathbf{J}_p = 0$ at the heated bottom wall; (b) $T = T_c$, $\mathbf{V} = 0$ and $\mathbf{J}_p = 0$ at the cooled top wall; and (c) $\partial T/\partial y = 0$, $\mathbf{V} = 0$ and $\mathbf{J}_p = 0$ at any adiabatic sidewall. The initial conditions presume that the nanofluid is

at rest, i.e., $\mathbf{V} = 0$, at uniform temperature, $T = T_c$, and at assigned uniform nanoparticles mass fraction, m_{av}.

Table 1. Physical properties of metal-oxide nanoparticles (at 25 °C) [6,36,37].

Nanoparticles	ρ (kg/m^3)	k (W/m K)	C_p (J/kg K)
Al$_2$O$_3$	3880	36	773
CuO	6500	17.6	540
TiO$_2$	4175	8.4	692

2.2. Computational Procedure

The system of Equations (1)–(4), with the boundary and initial conditions, is solved using the open source framework OpenFOAM [38]. A new solver, derived from the basic solver named *buoyantSimpleFoam* provided in OpenFOAM, has been developed with the implementation of the nanoparticle diffusion mass equation and assuming that all the physical properties of the nanofluid are temperature-dependent. The pressure–velocity coupling is solved by the SIMPLE algorithm, and all the convective terms are discretized using the QUICK scheme. The computational domain consists of a non-uniform structured grid, having a higher concentration of grid lines near the boundary walls of the enclosure and a uniform spacing in the interior of the cavity. Starting from the assigned initial conditions, the steady-state solution is attained when the relative changes at any computational node for each variable, between two consecutive iterations, are smaller than the pre-specified values of 10^{-6}.

At the steady-state, the heat transfer rates Q_h and Q_c at the heated and cooled walls are expressed by:

$$Q_h = \int_0^W -(k_n)_h \cdot \left. \frac{\partial T}{\partial y} \right|_{y=0} dx \tag{14}$$

$$Q_c = \int_0^W -(k_n)_c \cdot \left. \frac{\partial T}{\partial y} \right|_{y=H} dx \tag{15}$$

where $(k_n)_h$ and $(k_n)_c$ are the nanofluid thermal conductivities at temperatures T_h and T_c, respectively.

Since at steady-state the incoming and outgoing heat transfer rates are the same, the rate of heat transferred across the cavity can be calculated as:

$$Q_h = -Q_c = Q \tag{16}$$

Accordingly, the average convective heat transfer coefficient, h_{av}, is calculated as:

$$h_{av} = \frac{Q}{(T_h - T_c)W} \tag{17}$$

Numerical tests have been performed to analyze the sensitivity of the mesh spacing for several combinations of the controlling parameters, i.e., m_{av}, $\Delta T = T_h - T_c$, and $A = H/W$. In the rest of the discussion, the average nanoparticle volume fraction, φ_{av}, will be considered instead of m_{av}:

$$\varphi_{av} = \left[\left(\frac{1}{m_{av}} - 1 \right) \frac{\rho_s}{\rho_f} + 1 \right]^{-1} \tag{18}$$

where the mass densities ρ_s and ρ_f are evaluated at temperature T_{av}:

$$T_{av} = \frac{T_h + T_c}{2} \tag{19}$$

The typical number of nodal points $(x \times y)$ used for simulations are 100×100 for the square cavity and 200×100 for the cavity with aspect ratio $A = 0.25$, whereas the time-steps lie in the range between 10^{-3} s and 10^{-2} s. Typical results of the sensitivity analysis are presented in Tables 2 and 3.

Table 2. Grid sensitivity analysis for $H = 0.01$ m, $T_c = 300$ K, $\Delta T = 0.5$ K, $d_p = 25$ nm, $\Delta t = 1 \times 10^{-3}$ s.

A	φ_{av}	Mesh Size	Q (W)	φ_{max}	φ_{min}
1	0.01	40×40	0.661	0.00975	0.00930
		60×60	0.676	0.01007	0.00947
		80×80	0.687	0.01030	0.00966
		100×100	0.692	0.01040	0.00970
1	0.01	60×60	0.623	0.03950	0.03718
		80×80	0.641	0.04012	0.03802
		100×100	0.650	0.04059	0.03863
		120×120	0.656	0.04080	0.03890
0.25	0.04	120×60	2.731	0.03865	0.03710
		160×80	2.816	0.03955	0.03790
		200×100	2.891	0.04051	0.03836
		240×120	2.920	0.04070	0.03870

Table 3. Time-step sensitivity analysis for $H = 0.01$ m, $A = 0.25$, $T_c = 300$ K, $\Delta T = 0.5$ K, $\varphi_{av} = 0.04$, $d_p = 25$ nm.

Mesh Size	Δt (s)	Q (W)	φ_{max}	φ_{min}
200×100	5×10^{-2}	2.749	0.03843	0.03642
	1×10^{-2}	2.817	0.03954	0.03728
	5×10^{-3}	2.868	0.04015	0.03818
	1×10^{-3}	2.891	0.04051	0.03836

To validate the numerical code, two tests have been carried out. In the first test, the average Nusselt numbers computed numerically for a Prandtl number $Pr = 5.8$ (which means water at $T_{av} = 300$ K) and Rayleigh numbers $Ra = 10^3$–10^6, assuming $m_{av} = 0$ and $A = 0.5$, have been compared with the correlation of Hollands et al. [39] based on wide sets of experimental data for laminar free convection in cavities filled with air and water. In the second test, the experiments of Putra et al. [40], for a square cavity filled with $Al_2O_3 + H_2O$, have been reproduced for two different values of nanofluid volume fraction, $\varphi_{av} = 0.01$ and 0.04. The comparisons between our numerical solutions and the literature data are shown in Figures 2 and 3. Further details about the validation procedure can be found in [41].
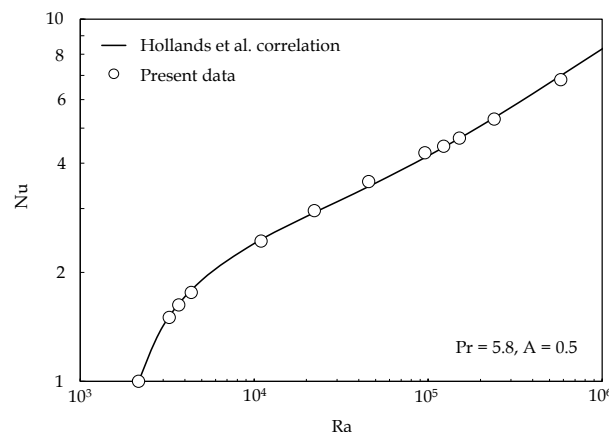

Figure 2. Comparison of the present results with the correlation of Hollands et al. [39] for water.
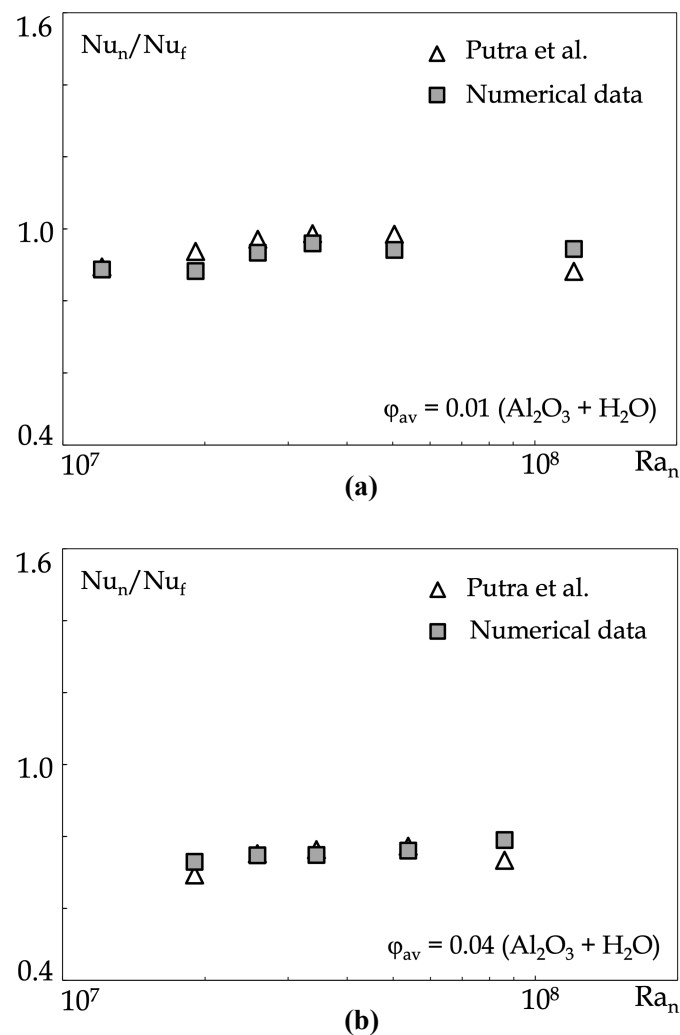
Figure 3. Comparison between the present numerical values and the corresponding data of Putra et al. [40] for $Al_2O_3 + H_2O$ in a differentially heated vertical enclosure: (**a**) $\varphi_{av} = 0.01$; (**b**) $\varphi_{av} = 0.04$.

3. Results

Numerical simulations are performed using $Al_2O_3 + H_2O$ nanofluid, for values of the volume fraction, φ_{av}, in the range between 0 and 0.04, and for values of the aspect ratio, $A = H/W$, in the range between 0.25 and 1. The height of the enclosure, H, the average diameter of the nanoparticles, d_p, and the temperature of the bottom wall have been fixed to 0.01 m, 25 nm, and 300 K, respectively, for all simulations. With these values, varying the temperature difference within the cavity, the Rayleigh number based on the height of the plate lies in the range between $5 \times 10^2 \leq Ra_n \leq 10^4$, in which the effective physical properties of the nanofluid are calculated at the average temperature and average volume fraction.

The more common way to present heat transfer results is the typical dimensionless distributions displayed in Figure 4, where the Nusselt number Nu is plotted versus Ra_n for a square cavity using the average volume fraction as a parameter. As expected, Nu increases for values of Ra_n above the critical value, Ra_c, corresponding to the departure from the perfectly conducting solution of a nanofluid static layer with an Nu value equal to unity. What seems important to point out is that the Nu-Ra data do not lie on a unique interpolation curve, which is what would be expected if the nanofluid should behave as a pure fluid, thus illuminating the two-phase behaviou of the nanofluids due to the Brownian motion and thermophoresis diffusion of the suspended nanoparticles, as already experimentally found by Putra et al. [40]

and Ho et al. [42] using Al_2O_3 + H_2O in cavities differentially heated at the sides. As clearly shown, the dispersion of a progressively larger amount of particles in mass flux into the base fluid seems to result in two main effects: an increase in Nu and a progressive reduction in the nanofluid layer's stability, with the consequent decrease in the critical Rayleigh number for the onset of convection. Actually, if the analysis is conducted considering the distributions of the average heat transfer coefficient h_{av} plotted versus the temperature difference ΔT imposed across the cavity for different values of the average volume fraction φ_{av}, as shown in Figure 5, it is evident that the heat transfer coefficient decreases when the average volume fraction is increased, while the value of ΔT corresponding to the onset of convection increases as the average volume fraction is increased, which is a direct consequence of the growth in the dynamic viscosity. Thus, it can be concluded that the dispersion of nanoparticles in the base fluid is detrimental for the heat transfer performance and that the nanofluid layer is more stable than the base fluid. The values of ΔT corresponding to the onset of convection, for water and alumina-water nanofluids with $\varphi_{av} = 0.01$ and $\varphi_{av} = 0.04$, are, respectively, 0.14 K, 0.16 K, and 0.2 K. Notice that the value assumed by the heat transfer coefficient h_{av} at the onset of convection corresponds to the theoretical conductance k/H of the stratified nanofluid layer. On account of the above considerations, it is clear that using a two-phase modeling, which permits us to account for the non-negligible slip effects occurring between suspended nanoparticles and base fluid, i.e., Brownian diffusion and, much more importantly, thermophoresis, makes the representation of the heat transfer performance not meaningful in terms of dimensionless parameters.
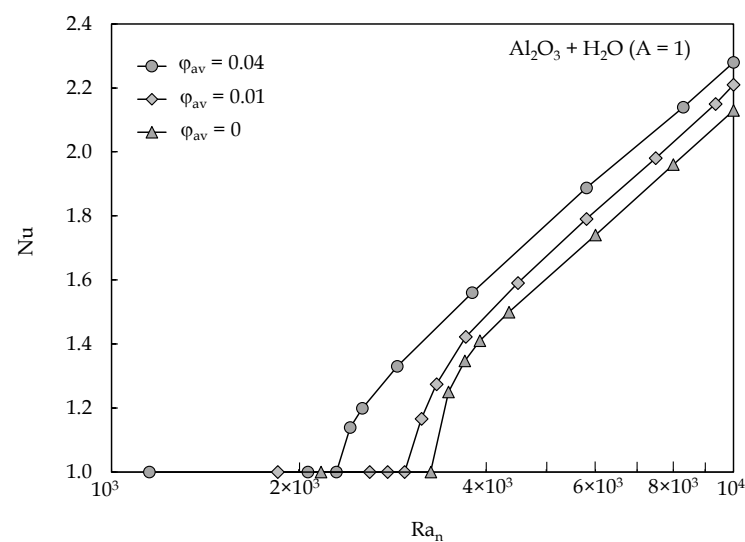

Figure 4. Distribution of Nu vs. Ra_n for $A = 1$, using φ_{av} as a parameter.

Selected local results to describe the time evolution from the onset of convection up to the steady-state solution are displayed in the sequence reported in Figure 6, in which the streamlines, the isotherm, and the isoconcentration contours are plotted for $A = 0.25$, $\varphi_{av} = 0.04$, and $\Delta T = 0.5$. As expected, the conductive solution is rapidly reached in the initial stages, whereas a longer time is needed before a number of weak convective solutal plumes start evolving from the heated bottom wall. Once the concentration field is sufficiently strong to penetrate the stratified thermal field, the upward movement of the nanoparticles by thermophoresis diffusion determines the thermal stratification breakdown and the growth of large circulatory roll-cells with the formation of hot and cold nanofluid jets traveling upwards and downwards within the cavity. This effect being strongly related to the buoyancy ratio, a pronounced reduction in the critical condition for the onset of convection has to be expected in comparison with the case of the single-phase approach, as shown in Figure 7.
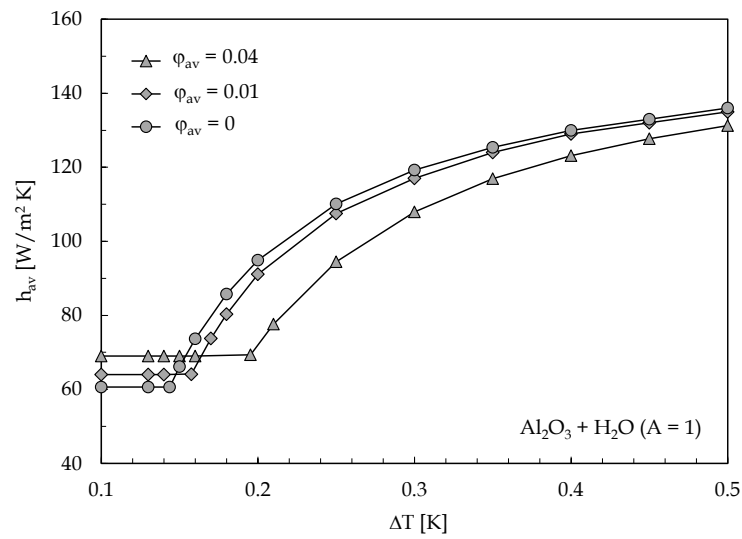
Figure 5. Distribution of h_{av} vs. ΔT for $A = 1$, using φ_{av} as a parameter.

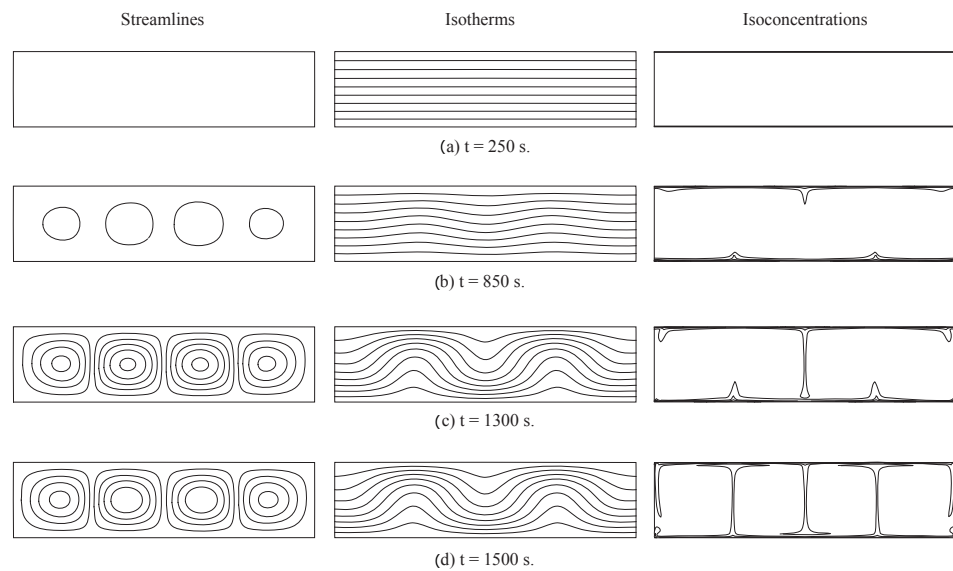**Figure 6.** Time evolution of streamlines, isotherms and isoconcentration contours for $Al_2O_3 + H_2O$ with $A = 0.25$, $\varphi_{av} = 0.4$ and $\Delta T = 0.15$.
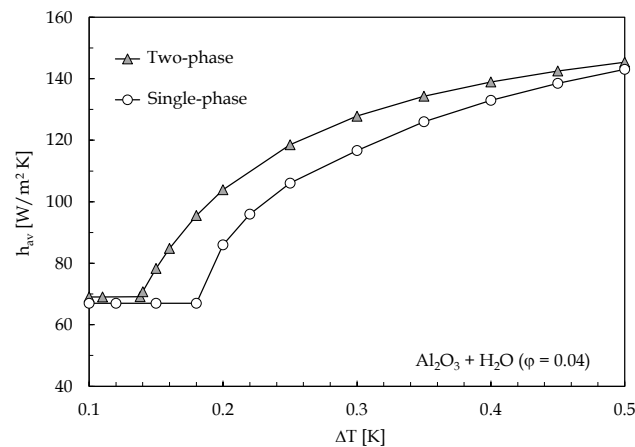

Figure 7. Distribution of h_{av} vs. ΔT for $A = 0.25$, obtained using single-phase approach and two-phase approach.

Distributions of the heat transfer coefficient h_{av} for the base fluid and the nanofluid using the aspect ratio A as a parameter are plotted in Figures 8 and 9. It can be noticed that the ΔT corresponding to the onset of convection decreases with decreasing the aspect ratio of the cavity. This is due to the progressively more negligible influence of the fluid confinement at the sidewalls for effect of the viscosity. The smaller is the aspect ratio of the enclosure, the larger is the movement capacity of the fluid with consequent enhancement of the heat transfer rate. Moreover, the difference between nanofluid and base fluid tends to reduce due to the cooperating downward solutal driving force, which has the beneficial effect to compensate the increased viscosity, as shown in Figure 10.
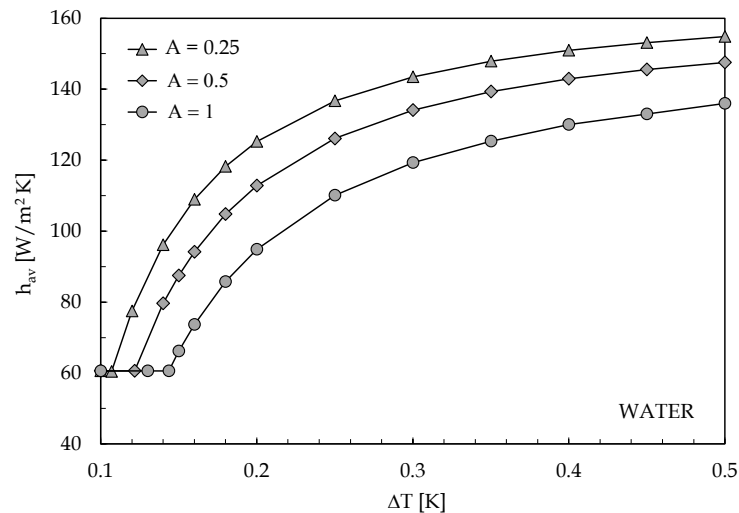

Figure 8. Distribution of h_{av} vs. ΔT for water, using A as a parameter.
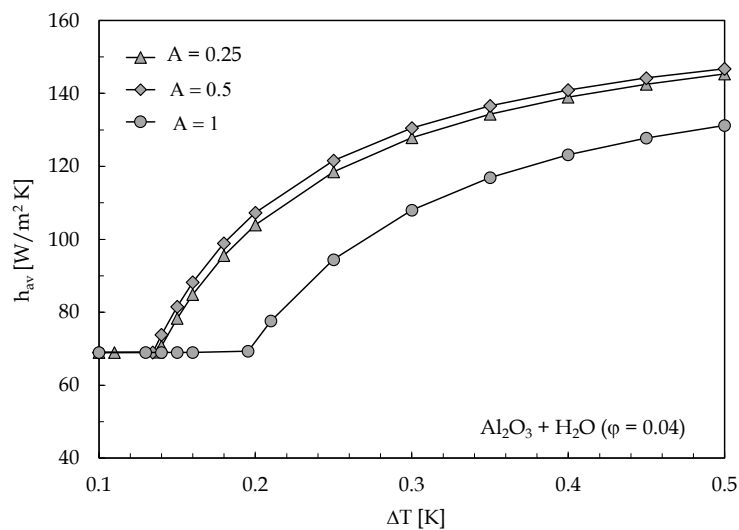

Figure 9. Distribution of h_{av} vs. ΔT for $Al_2O_3 + H_2O$, $\varphi_{av} = 0.04$, using A as a parameter.

Finally, as far as the role of the nanoparticle material is concerned, its effect on the onset conditions is displayed in Figure 10, where the values of h_{av} for three different nanofluids, $Al_2O_3 + H_2O$, $CuO + H_2O$, and $TiO_2 + H_2O$, have been reported for $A = 1$ and $\varphi_{av} = 0.01$. It is worth pointing out that the onset of convection is anticipated for $TiO_2 + H_2O$ than for $CuO + H_2O$ and $Al_2O_3 + H_2O$ due to the higher value of S_T.
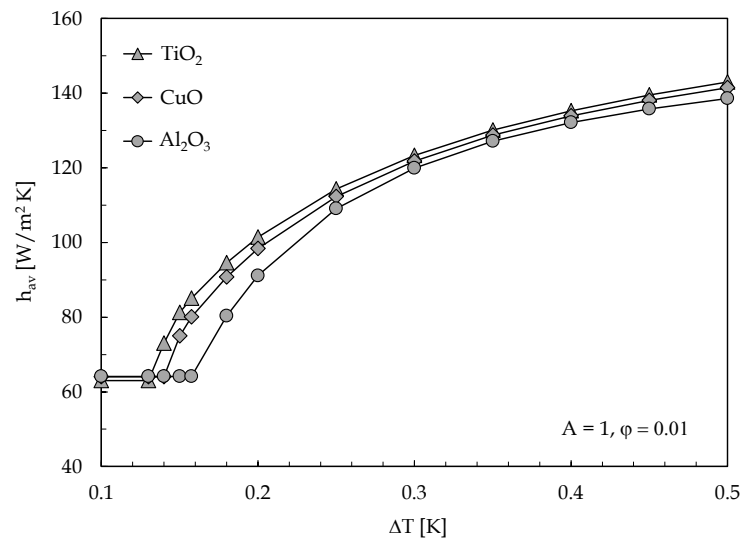
Figure 10. Distribution of h_{av} vs. ΔT for a $A = 1$, using different nanoparticle materials.

4. Conclusions

Natural convection in a rectangular enclosure filled with nanofluid and heated from below is studied numerically using a two-phase model based on the double-diffusive approach, considering that the slip mechanisms between liquid and solid phases are only due to the Brownian diffusion and thermophoresis.

Simulations have been performed using $Al_2O_3 + H_2O$ for different values of the average volume fraction of the suspended solid phase, and for different aspect ratio of the cavity, with the scope to investigate how the onset of convection is affected by the presence of the nanoparticles dispersed into the base fluid, also taking into account the lateral confinement effect.

The results may be summarized as follows:

1. The value of the difference in temperature ΔT between the heated and cooled horizontal walls corresponding to the onset of convection increases as the average volume fraction is increased, which is a consequence of the growth of the dynamic viscosity;
2. The nanoparticles migration from hot to cold results in a pronounced reduction in the critical condition for the onset of convection in comparison with the case of the single-phase approach;
3. The value of the difference of temperature ΔT corresponding to the onset of convection decreases with decreasing the aspect ratio of the cavity;
4. The onset of convection is anticipated for $TiO_2 + H_2O$ than for $CuO + H_2O$ and $Al_2O_3 + H_2O$, due to the higher value of thermophoresis parameter S_T.

The above results represent the first analysis of a wider investigation bearing on the instability of nanofluid layers in a cavity. In the future, further numerical works will be proposed in order to extend the present research to three-dimensional cases.

References

1. Wen, D.; Ding, Y. Natural convective heat transfer of suspensions of titanium dioxide nanoparticles (nanofluids). *IEEE Trans. Nanotechnol.* **2006**, *5*, 220–227.
2. Rao, S.; Srivastava, A. Interferometric study of natural convection in a differentially-heated cavity with Al_2O_3–water based dilute nanofluids. *Int. J. Heat Mass Transf.* **2016**, *92*, 1128–1142. [CrossRef]
3. Chang, B.H.; Mills, A.F.; Hernandez, E. Natural convection of microparticles suspensions in thin enclosures. *Int. J. Heat Mass Transf.* **2008**, *51*, 1332–1341. [CrossRef]
4. Hwang, K.S.; Lee, J.; Jang, S.P. Buoyancy-driven heat transfer of water-based Al_2O_3 nanofluids in a rectangular cavity. *Int. J. Heat Mass Transf.* **2007**, *50*, 4003–4010. [CrossRef]
5. Jang, S.P.; Choi, S.U.S. The role of Brownian motion in the enhanced thermal conductivity of nanofluids. *Appl. Phys. Lett.* **2004**, *84*, 4316–4318. [CrossRef]
6. Pak, B.C.; Cho, Y. Hydrodynamic and heat transfer study of dispersed fluids with submicron metallic oxide particle. *Exp. Heat Transf.* **1998**, *11*, 151–170. [CrossRef]
7. Park, H.M. Rayleigh-Benard convection of nanofluids based on the pseudo-single-phase continuum model. *Int. J. Therm. Sci.* **2015**, *90*, 267–278. [CrossRef]
8. Kim, J.; Kang, Y.T.; Choi, C.K. Analysis of convective instability and heat transfer characteristics of nanofluids. *Phys. Fluids* **2004**, *16*, 2395. [CrossRef]
9. Tzou, D.Y. Thermal instability of nanofluids in natural convection. *Int. J. Heat Mass Transf.* **2008**, *51*, 2967–2979. [CrossRef]
10. Tzou, D.Y. Instability of nanofluids in natural convection. *J. Heat Transf.* **2008**, *130*, 072401. [CrossRef]
11. McNab, G.S.; Meisen, A. Thermophoresis in liquids. *J. Colloid Interf. Sci.* **1973**, *44*, 339–346. [CrossRef]
12. Ryskin, A.; Muller, H.W.; Pleiner, H. Thermal convection in binary fluid mixtures with a weak concentration diffusivity, but strong solutal buoyancy forces. *Phys. Rev. E* **2003**, *67*, 046302. [CrossRef] [PubMed]
13. Nield, D.A.; Kuznetsov, A.V. The effect of local thermal nonequilibrium on the onset of convection in a nanofluid. *J. Heat Transf.* **2010**, *132*, 052405. [CrossRef]
14. Nield, D.A.; Kuznetsov, A.V. The onset of double-diffusive convection in a nanofluid layer. *Int. J. Heat Fluid Flow* **2011**, *32*, 771–776. [CrossRef]
15. Nield, D.A.; Kuznetsov, A.V. The onset of convection in a nanofluid layer of finite depth: A revised model. *Int. J. Heat Mass Transf.* **2014**, *77*, 915–918. [CrossRef]
16. Nield, D.A.; Kuznetsov, A.V. The onset of convection in an internally heated nanofluid layer. *J. Heat Transf.* **2014**, *136*, 014501. [CrossRef]
17. Agarwal, S.; Rana, P.; Bhadauria, B.S. Rayleigh–Benard convection in a nanofluid layer using a thermal nonequilibrium model. *J. Heat Transf.* **2014**, *136*, 122501. [CrossRef]
18. Haddad, Z.; Abu-Nada, E.; Oztop, H.F.; Mataoui, A. Natural convection in nanofluids: Are the thermophoresis and Brownian motion effects significant in nanofluid heat transfer enhancement? *Int. J. Therm. Sci.* **2012**, *57*, 152–162. [CrossRef]
19. Ho, C.J.; Chen, D.; Yan, W.; Mahian, O. Rayleigh–Bénard convection of Al_2O_3/water nanofluids in a cavity considering sedimentation, thermophoresis, and Brownian motion. *Int. Commun. Heat Mass Transf.* **2014**, *57*, 22–26. [CrossRef]
20. Eslamian, M.; Ahmed, M.; El-Dosoky, M.F.; Saghir, M.Z. Effect of thermophoresis on natural convection in a Rayleigh–Benard cell filled with a nanofluid. *Int. J. Heat Mass Transf.* **2015**, *81*, 142–156. [CrossRef]
21. Savithiri, S.; Pattamatta, A.; Das, S. Rayleigh–Benard convection in water-based alumina nanofluid: A numerical study. *Numer. Heat Transf. Part A* **2017**, *71* 202–214. [CrossRef]
22. Sun, M.; Wang, G.; Zhang, X. Rayleigh-Bénard convection of non-Newtonian nanofluids considering Brownian motion and thermophoresis. *Int. J. Therm. Sci.* **2019**, *139*, 312–325. [CrossRef]
23. Ahuja, J.; Sharma, J. Rayleigh-Bénard instability in nanofluids: A comprehensive review. *Micro Nano Syst. Lett.* **2020**, *8*, 1–15. [CrossRef]
24. Buongiorno, J. Convective transport in nanofluids. *J. Heat Transf.* **2006**, *128*, 240–250. [CrossRef]
25. Das, S.K.; Putra, N.; Roetzel, W. Pool boiling characteristics of nano-fluids. *Int. J. Heat Mass Transf.* **2003**, *46*, 851–862. [CrossRef]
26. Prasher, R.; Song, D.; Wang, J.; Phelan, P. Measurements of nanofluid viscosity and its implications for thermal applications. *Appl. Phys. Lett.* **2006**, *89*, 133108. [CrossRef]
27. He, Y.; Jin, Y.; Chen, H.; Ding, Y.; Cang, D.; Lu, H. Heat transfer and flow behaviour of aqueous suspensions of TiO_2 nanoparticles (nanofluids) flowing upward through a vertical pipe. *Int. J. Heat Mass Transf.* **2007**, *50*, 2272–2281. [CrossRef]
28. Chen, H.; Ding, Y.; He, Y.; Tan, C. Rheological behaviour of ethylene glycol based titania nanofluids. *Chem. Phys. Lett.* **2007**, *444*, 333–337. [CrossRef]
29. Chevalier, J.; Tillement, O.; Ayela, F. Rheological properties of nanofluids flowing through microchannels. *Appl. Phys. Lett.* **2007**, *91*, 233103. [CrossRef]
30. Cabaleiro, D.; Pastoriza-Gallego, M.J.; Piñero, M.M.; Lugo, L. Characterization and measurements of thermal conductivity, density and rheological properties of zinc oxide nanoparticles dispersed in (ethane-1,2-diol + water) mixture. *J. Chem. Thermodyn.* **2013**, *58*, 405–415. [CrossRef]
31. Einstein, A. Über die von der molekularkinetischen Theorie der Wärme geforderte Bewegung von in ruhenden Flüssigkeiten suspendierten Teilchen. *Ann. Phys.* **1905**, *17*, 549–560. [CrossRef]

32. Brenner, H.; Bielenberg, J.R. A continuum approach to phoretic motions: Thermophoresis. *Physica A* **2005**, *355*, 251–273. [CrossRef]

33. Corcione, M.; Cianfrini, M.; Quintino, A. Enhanced natural convection heat transfer of nanofluids in enclosures with two adjacent walls heated and the two opposite walls cooled. *Int. J. Heat Mass Transf.* **2015**, *88*, 902–913. [CrossRef]

34. Corcione, M. Empirical correlating equations for predicting the effective thermal conductivity and dynamic viscosity of nanofluids. *Energy Convers. Manag.* **2011**, *52*, 789–793. [CrossRef]

35. Linstrom, P.J.; Mallard, W.G. *NIST Chemistry WebBook*; NIST Standard Reference Database Number 69; National Institute of Standards and Technology: Gaithersburg, MD, USA, 2022. Available online: http://webbook.nist.gov (accessed on 10 December 2021).

36. Das, S.K.; Putra, N.; Thiesen, P.; Roetzel, W. Temperature dependence of thermal conductivity enhancement for nanofluids. *J. Heat Transf.* **2003**, *125*, 567–574. [CrossRef]

37. Mintsa, H.A.; Roy, G.; Nguyen, C.T.; Doucet, D. New temperature dependent thermal conductivity data for water-based nanofluids. *Int. J. Therm. Sci.* **2009**, *48*, 363–371. [CrossRef]

38. Greenshields, C. *OpenFOAM User Guide*; Version 8; OpenFOAM Foundation Ltd.: Reading, UK, 2022.

39. Hollands, K.G.T.; Raithby, G.D.; Konicek, L. Correlation equations for free convection heat transfer in horizontal layers of air and water. *Int. J. Heat Mass Transf.* **1975**, *18*, 879–884. [CrossRef]

40. Putra, N.; Roetzel, W.; Das, S.K. Natural convection of nano-fluids. *Heat Mass Transf.* **2003**, *39*, 775–784. [CrossRef]

41. Corcione, M.; Cianfrini, M.; Quintino, A. Temperature effects on the enhanced or deteriorated buoyancy-driven heat transfer in differentially heated enclosures filled with nanofluids. *Numer. Heat Transf. Part A* **2016**, *70*, 223–241. [CrossRef]

42. Ho, C.J.; Liu, Y.S.; Chang, Y.S.; Lin, C.C. Natural convection heat transfer of alumina-water nanofluid in vertical square enclosures: An experimental study. *Int. J. Therm. Sci.* **2010**, *49*, 1345–1353. [CrossRef]